ECCOMAS Multibody Dynamics 2013
1-4 July, 2013, University of Zagreb, Croatia

A Multibody Model to Assess the Effect of Automotive Motor In-wheel Configuration on Vehicle Stability and Comfort

Javier Cuadrado[1], David Vilela[1], Iñaki Iglesias[2], Adrián Martín[2], Alberto Peña[2]

[1] Laboratorio de Ingeniería Mecánica, University of La Coruña, Escuela Politécnica Superior, Mendizábal s/n, 15403 Ferrol, Spain: javicuad@cdf.udc.es,david.vilela@udc.es
[2] Industry and Transport Division, Tecnalia Research and Innovation, Parque Tecnológico de Bizkaia, Ibaizabal Bidea, Edif. 202, 48170 Zamudio, Spain: {inaki.iglesias,adrian.martin,alberto.pena}@tecnalia.com

Abstract

Motor in-wheel topology is an optional configuration for electric-powered vehicles which has some advantages over the conventional standalone motor configuration, like improved modularity when designing different drivetrains (FWD, RWD, AWD) and increased usable interior space of the vehicle. However, drawbacks are also present due to the added unsprung mass, which directly affects to vehicle road holding and ride comfort, and may increase the suspension design cycle, as there is no data available from similar designs. In this work, a multibody model of a B-class car has been developed in order to assess the effect of motor in-wheel configuration on vehicle stability and comfort. The car is modeled in relative coordinates, being the suspensions described as macro-joints by means of lookup tables thus yielding a tree-like structure, and a semi-recursive formulation is applied to derive the equations of motion, which are numerically integrated in time through the trapezoidal rule. Three tests are carried out to compare the behavior of conventional and motor in-wheel configurations: sine sweep, obstacle avoidance and constant radius. A number of motion indicators are obtained from these maneuvers so as to measure the ride, handling and steering characteristics.

Keywords: *electric vehicle, motor in-wheel, unsprung mass, vehicle stability and comfort, ride and handling, open-loop model, relative coordinates, lookup tables, semi-recursive formulation*

1 Introduction

Research in electric-powered vehicles has notably increased in the last years [1]. The new propulsion system brings up a lot of questions and challenges but, on the other hand, opens new design alternatives. This is for example the case of motor in-wheel topology, shown in figure 1, which has many advantages over more traditional designs using standalone motor configuration with one differential for the whole transmission drivetrain. Improved modularity when designing different drivetrains (FWD, RWD, AWD), increased usable interior space of the vehicle, and the potential application of torque control for improved handling by means of torque vectoring techniques, are the main advantages generating interest and development effort from many OEM's.

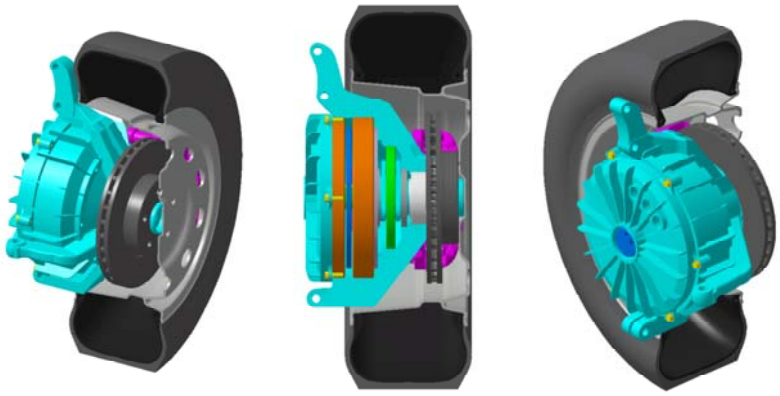

Figure 1. Three views of a motor in-wheel system.

At the same time, motor in-wheel technology presents some deficiencies, being critical the added unsprung mass over the conventional design. Unsprung mass directly affects to vehicle road holding and ride comfort and, even if recent empirical studies have shown that this mass increase does not substantially affect vehicle behaviour [2], the ride

comfort, which is one of the strong key aspects of the electric vehicle, is degraded. Moreover, motor in-wheel suspension uniqueness in terms of added unsprung mass, increases the suspension design cycle, as there is no data available from similar designs.

Simulation can help to study all the mentioned aspects. In this work, a multibody model of a B-class car has been developed, so as to allow the suspension designer to study the effect of the motor in-wheel configuration on the vehicle stability and comfort. The car is modeled with relative coordinates and the mass matrix and force vector of the multibody system are recursively obtained [3]. Each suspension is considered as a macro-joint by means of lookup tables [4], thus leading to a tree-like configuration mechanism with no closed loops. The motor in-wheel system is modeled as a point mass added to the knuckle, since the rotating components in motor and gearbox possess very low mass. The implicit single-step trapezoidal rule is used to integrate in time the independent relative coordinates.

The resulting formulation is fast and robust, so that violent maneuvers can be performed as required by the tests later described, while the execution times are kept within real-time performance, thus even allowing to carry out hardware-in-the-loop simulations if desired, an interesting feature for the future development of control algorithms for torque vectoring. Moreover, the use of macro-joints streamlines the designer's work, since changes in suspension topology and/or parameters are easily introduced by simply updating the lookup tables.

In order to assess the quality of a given solution, the ride, handling and steering characteristics should be analyzed. Maneuvers must be defined, seeking to identify the indicators which are more affected by the increase in unsprung mass as well as those which can be perceived by the customers as detrimental. As ride characteristics, impact feel and pitch control have been considered, which can be measured through chassis vertical acceleration and pitch angle histories, respectively, during a sine sweep test (ISO 2631: 2004). Regarding handling characteristics, stability can be deducted from the histories of yaw and roll angles in an obstacle avoidance test (ISO 3888: 2002), while under/oversteer balance can be determined from a handling diagram in a constant radius test (ISO 4138: 2004). The steering characteristics, effort level and linearity, can also be measured in the constant radius test.

The remaining of the paper is organized as follows. Section 2 describes the car and its modeling, including the use of macro-joints at the suspensions. Section 3 explains the semi-recursive formulation and the integration of the equations of motion. Section 4 presents the three tests that have been conducted along with the results obtained for the selected indicators in the cases of conventional and motor in-wheel configurations. Finally, section 5 gathers the conclusions of the work.

2 The car and the model

The concept demostrator vehicle that has been considered in this study is a Fiat Punto, a typical B-segment car. Figure 2a shows the external appearance of the vehicle, while figure 2b shows the internal components and recreates a possible adaptation as electric vehicle. The front suspension is of McPherson type, while a twist-beam system is mounted in the rear part. Some basic parameters of the car model are listed in Table 1.

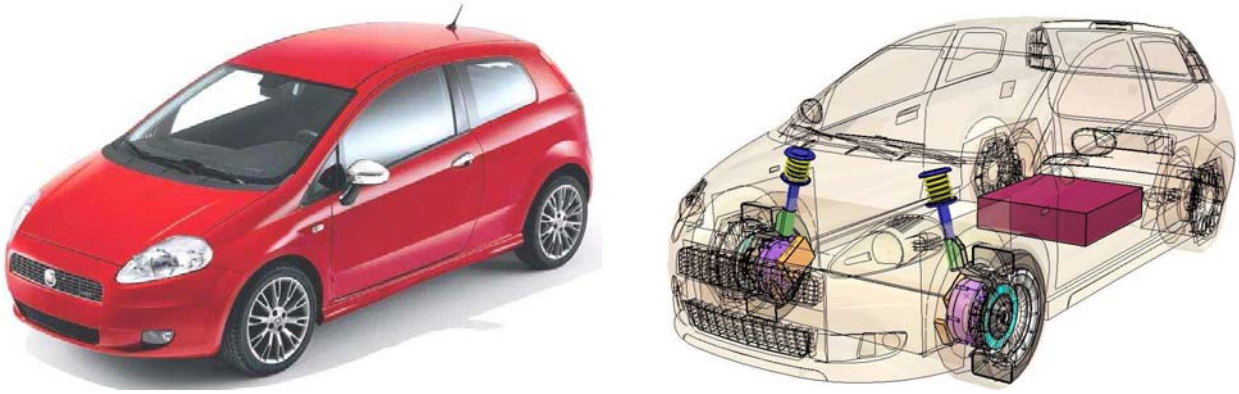

Figure 2. Fiat Punto: a) External appearance; b) Possible adaptation as electric vehicle.

Relative coordinates have been used for the modeling. The three Cartesian coordinates of a chassis point in the front part of the car, (x, y, z), along with the three Cardan angles of the chassis with respect to the inertial frame of reference (α, β, γ), are the six independent coordinates defining the chassis position. The travel of each suspension is defined by the local (with respect to the chassis reference frame) vertical Cartesian coordinate of the wheel center, $\bar{z}_i (i = 1:4)$. By solving the suspension kinematics, a table is generated which provides, for every value of the mentioned suspension coordinate, the three local Cartesian coordinates of the knuckle/wheel center and the three local Cardan angles of the knuckle reference frame. Finally, the position of each wheel with respect to the knuckle is defined by an angle around the wheel axis, $\varphi_i (i = 1:4)$. This makes a total of fourteen independent coordinates, which are grouped into vector **z**.

$$\mathbf{z}^{\mathrm{T}} = \{x \quad y \quad z \quad \alpha \quad \beta \quad \gamma \quad \bar{z}_1 \quad \bar{z}_2 \quad \bar{z}_3 \quad \bar{z}_4 \quad \varphi_1 \quad \varphi_2 \quad \varphi_3 \quad \varphi_4\}. \tag{1}$$

The steering coordinate is also provided, but it is not included in the list of coordinates, since the steering motion is imposed; then, for the front suspensions, a different table is generated for every different value of the steering coordinate. Table data are generated, either for the travelling and steering motions, with a resolution of 1 mm in the corresponding input coordinate (local vertical Cartesian coordinate of the wheel center and steering-rack distance, respectively), the output values being linearly interpolated. Regarding the rear suspensions, corrections are introduced to the knuckle orientation provided by the table to better reproduce the twin beam action: camber and toe corrections are obtained as linear functions of the rolling angle of the vehicle. It must be noted that the resulting model possesses a tree-like topology with no closed loops, as illustrated in figure 3.

Table 1. Basic parameters of the car model.

Wheelbase	2.51 m	Front suspension damping	8,533 Ns/m
Front and rear track	1.50 m	Anti-roll beam stiffness	10,000 N/m
Chassis mass	955 kg	Rear suspension stiffness	39,240 N/m
Front knuckle mass	12.5 kg	Rear suspension damping	5,138 Ns/m
Rear knuckle mass	32.5 kg	Twist beam roll stiffness	10,000 N/m
Wheel mass	17.5 kg	Tire radius	315.9 mm
Front suspension stiffness	58,860 N/m	Tire stiffness	237,000 N/m

Going now to the applied forces, the mass and, hence, the weight, has only been considered for the chassis, knuckles and wheels. The motor in-wheel configuration has been taken into account by simply incrementing the mass of the front wheels in 30 kg each. Since the suspension links have not been modeled but substituted by the already described lookup tables, the forces due to the spring-damper elements in the suspensions have been introduced through the motion-ratio approach [5]. Furthermore, either the front anti-roll beam and the rear twist beam actuation is simulated by appling forces to the right and left wheels which oppose their relative local vertical motion. Tire radial stiffness has been modeled by means of a linear spring, while lateral and longitudinal tire forces follow a third order polinomial function of the corresponding input magnitude (slip angle and slip ratio, respectively) until a certain limit value for which saturation is reached; later, the total tangential force is calculated and saturation is checked again, being the lateral and longitudinal components corrected in case the maximum allowable force is exceeded. In order to determine the contact parameters (contact point, normal direction and indentation), a collision detection algorithm has been implemented which considers a cylindrical bounding volume for each wheel and checks its collision against the triangular mesh describing the ground or road.

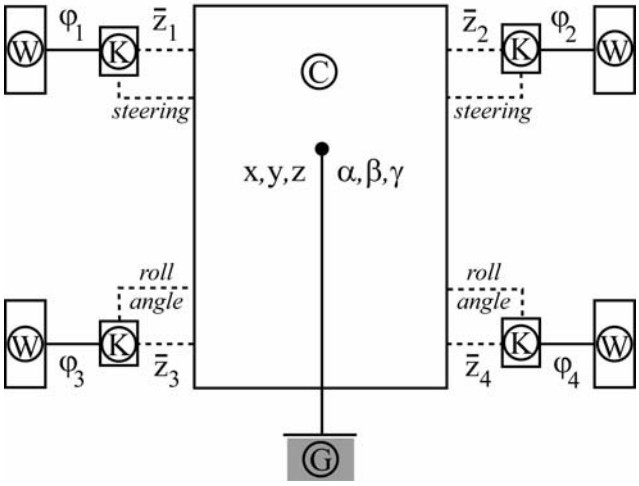

Figure 3. Kinematic structure of the car model. G: ground; C: chassis; K: knuckle; W: wheel. Dotted lines: lookup tables.

3 Dynamic formulation and numerical integration

The semi-recursive dynamic formulation proposed in [3] has been used to derive the equations of motion of the car model. The formulation is general, in the sense that it can deal with systems containing either open or closed loops, so that dependent coordinates and constraint equations relating them are expected. However, in the present case the system possesses a tree-like kinematic structure, and a set of independent coordinates **z** has been defined, as previously

indicated. This means that the formulation becomes simpler, since no constraint equations must be considered.

At a certain instant of time, it is assumed that the independent positions $\mathbf{z}$ and velocities $\dot{\mathbf{z}}$ are known. Then, the tree kinematic structure is travelled from the root to the leaves in order to obtain the positions and velocities of points, and the rotation matrices and angular velocities of bodies. In the same journey, accelerations of points and angular accelerations of bodies are obtained for a virtual null value of the independent accelerations $\ddot{\mathbf{z}}$.

Such calculations are performed through the kinematic methods of classical Mechanics, and no particular remark is required to be done, except for the case of macro-joints substituting the suspension links. In that case, the vector of Cartesian coordinates of the origin of the knuckle local reference frame (for knuckle *i*, with suspension coordinate $\bar{z}_i$), $\mathbf{r}_\mathrm{k}$, is obtained as,

$$\mathbf{r}_\mathrm{k} = \mathbf{r}_\mathrm{c} + \mathbf{R}_\mathrm{c}\bar{\mathbf{r}}_\mathrm{k} \,. \tag{2}$$

where $\mathbf{r}_\mathrm{c}$ is the vector of Cartesian coordinates of the origin of the chassis local reference frame, (x, y, z), $\mathbf{R}_\mathrm{c}$ is the chassis rotation matrix, function of (α, β, γ), and $\bar{\mathbf{r}}_\mathrm{k}$ is the vector of local (with respect to the chassis reference frame) Cartesian coordinates of the point. This last vector is function of the respective suspension coordinate $\bar{z}_i$, and its coordinates $(\bar{x}, \bar{y}, \bar{z})$ are tabulated as functions of $\bar{z}_i$. As for the knuckle rotation matrix, $\mathbf{R}_\mathrm{k}$,

$$\mathbf{R}_\mathrm{k} = \mathbf{R}_\mathrm{c}\mathbf{R}_\mathrm{k/c} \,. \tag{3}$$

being $\mathbf{R}_\mathrm{k/c}$ the rotation matrix of the knuckle with respect to the chassis. This matrix is also function of the respective suspension coordinate $\bar{z}_i$, and its corresponding Cardan angles $(\bar{\alpha}, \bar{\beta}, \bar{\gamma})$ are tabulated as functions of $\bar{z}_i$. The form of $\mathbf{R}_\mathrm{k/c}$ is the well-known form of the rotation matrix when Cardan angles are used,

$$\mathbf{R}_\mathrm{k/c} = \begin{bmatrix} \cos\bar{\beta}\cos\bar{\gamma} & -\cos\bar{\beta}\sin\bar{\gamma} & \sin\bar{\beta} \\ \cos\bar{\alpha}\sin\bar{\gamma} + \sin\bar{\alpha}\sin\bar{\beta}\cos\bar{\gamma} & \cos\bar{\alpha}\cos\bar{\gamma} - \sin\bar{\alpha}\sin\bar{\beta}\sin\bar{\gamma} & -\sin\bar{\alpha}\cos\bar{\beta} \\ \sin\bar{\alpha}\sin\bar{\gamma} - \cos\bar{\alpha}\sin\bar{\beta}\cos\bar{\gamma} & \sin\bar{\alpha}\cos\bar{\gamma} + \cos\bar{\alpha}\sin\bar{\beta}\sin\bar{\gamma} & \cos\bar{\alpha}\cos\bar{\beta} \end{bmatrix} . \tag{4}$$

At velocity level, the expressions are, for the velocity of the origin of the knuckle local reference frame, $\mathbf{v}_\mathrm{k}$,

$$\mathbf{v}_\mathrm{k} = \mathbf{v}_\mathrm{c} + \boldsymbol{\omega}_\mathrm{c} \times (\mathbf{r}_\mathrm{k} - \mathbf{r}_\mathrm{c}) + \mathbf{R}_\mathrm{c} \frac{\mathrm{d}\bar{\mathbf{r}}_\mathrm{k}}{\mathrm{d}\bar{z}_i} \dot{\bar{z}}_i \,. \tag{5}$$

where $\mathbf{v}_\mathrm{c}$ is the velocity of the origin of the chassis local reference frame, and $\boldsymbol{\omega}_\mathrm{c}$ is the chassis angular velocity. The three components of the derivative of $\bar{\mathbf{r}}_\mathrm{k}$ with respect to $\bar{z}_i$ are tabulated as functions of $\bar{z}_i$. The knuckle angular velocity, $\boldsymbol{\omega}_\mathrm{k}$, is,

$$\boldsymbol{\omega}_\mathrm{k} = \boldsymbol{\omega}_\mathrm{c} + \mathbf{R}_\mathrm{c}\bar{\boldsymbol{\omega}}_\mathrm{k/c} \,. \tag{6}$$

being $\bar{\boldsymbol{\omega}}_\mathrm{k/c}$ the angular velocity of the knuckle with respect to the chassis, whose form is also well-known when Cardan angles are used,

$$\bar{\boldsymbol{\omega}}_\mathrm{k/c} = \begin{bmatrix} 1 & 0 & \sin\bar{\beta} \\ 0 & \cos\bar{\alpha} & -\sin\bar{\alpha}\cos\bar{\beta} \\ 0 & \sin\bar{\alpha} & \cos\bar{\alpha}\cos\bar{\beta} \end{bmatrix} \begin{Bmatrix} \dot{\bar{\alpha}} \\ \dot{\bar{\beta}} \\ \dot{\bar{\gamma}} \end{Bmatrix} . \tag{7}$$

Grouping the three Cardan angles defining the orientation of the knuckle with respect to the chassis as $\bar{\boldsymbol{\theta}}_\mathrm{k}^\mathrm{T} = \{\bar{\alpha} \quad \bar{\beta} \quad \bar{\gamma}\}$, and calling $\bar{\mathbf{A}}_\mathrm{k}$ the 3x3 matriz of equation (7), equation (6) can be further developed as

$$\boldsymbol{\omega}_\mathrm{k} = \boldsymbol{\omega}_\mathrm{c} + \mathbf{R}_\mathrm{c}\bar{\mathbf{A}}_\mathrm{k} \frac{\mathrm{d}\bar{\boldsymbol{\theta}}_\mathrm{k}}{\mathrm{d}\bar{z}_i} \dot{\bar{z}}_i \,. \tag{8}$$

which is quite similar to equation (5) for the translational terms. The three components of the derivative of $\bar{\boldsymbol{\theta}}_\mathrm{k}$ with respect to $\bar{z}_i$ are tabulated as functions of $\bar{z}_i$.

At acceleration level, the expressions are, for the acceleration of the origin of the knuckle local reference frame, $\mathbf{a}_\mathrm{k}$,

$$\mathbf{a}_\mathrm{k} = \mathbf{a}_\mathrm{c} + \boldsymbol{\alpha}_\mathrm{c} \times (\mathbf{r}_\mathrm{k} - \mathbf{r}_\mathrm{c}) + \boldsymbol{\omega}_\mathrm{c} \times \left[\boldsymbol{\omega}_\mathrm{c} \times (\mathbf{r}_\mathrm{k} - \mathbf{r}_\mathrm{c})\right] + 2\boldsymbol{\omega}_\mathrm{c} \times \mathbf{R}_\mathrm{c} \frac{\mathrm{d}\bar{\mathbf{r}}_\mathrm{k}}{\mathrm{d}\bar{z}_i} \dot{\bar{z}}_i + \mathbf{R}_\mathrm{c} \left(\frac{\mathrm{d}\bar{\mathbf{r}}_\mathrm{k}}{\mathrm{d}\bar{z}_i} \ddot{\bar{z}}_i + \frac{\mathrm{d}^2\bar{\mathbf{r}}_\mathrm{k}}{\mathrm{d}\bar{z}_i^2} \dot{\bar{z}}_i^2 \right) . \tag{9}$$

where $\mathbf{a}_\mathrm{c}$ is the acceleration of the origin of the chassis local reference frame, and $\boldsymbol{\alpha}_\mathrm{c}$ is the chassis angular acceleration. The three components of the second derivative of $\bar{\mathbf{r}}_\mathrm{k}$ with respect to $\bar{z}_i$ are tabulated as functions of $\bar{z}_i$.

The knuckle angular acceleration, $\boldsymbol{\alpha}_k$, is,

$$\boldsymbol{\alpha}_k = \boldsymbol{\alpha}_c + \mathbf{R}_c \bar{\boldsymbol{\alpha}}_{k/c} + \boldsymbol{\omega}_c \times \mathbf{R}_c \bar{\boldsymbol{\omega}}_{k/c} \,. \tag{10}$$

being $\bar{\boldsymbol{\alpha}}_{k/c}$ the angular acceleration of the knuckle with respect to the chassis, obtained as the time derivative of $\bar{\boldsymbol{\omega}}_{k/c}$ provided in equation (7),

$$\bar{\boldsymbol{\alpha}}_{k/c} = \begin{bmatrix} 1 & 0 & \sin\bar{\beta} \\ 0 & \cos\bar{\alpha} & -\sin\bar{\alpha}\cos\bar{\beta} \\ 0 & \sin\bar{\alpha} & \cos\bar{\alpha}\cos\bar{\beta} \end{bmatrix} \begin{Bmatrix} \ddot{\bar{\alpha}} \\ \ddot{\bar{\beta}} \\ \ddot{\bar{\gamma}} \end{Bmatrix} + \begin{bmatrix} 0 & 0 & \dot{\bar{\beta}}\cos\bar{\beta} \\ 0 & -\dot{\bar{\alpha}}\sin\bar{\alpha} & -\dot{\bar{\alpha}}\cos\bar{\alpha}\cos\bar{\beta} + \dot{\bar{\beta}}\sin\bar{\alpha}\sin\bar{\beta} \\ 0 & \dot{\bar{\alpha}}\cos\bar{\alpha} & -\dot{\bar{\alpha}}\sin\bar{\alpha}\cos\bar{\beta} - \dot{\bar{\beta}}\cos\bar{\alpha}\sin\bar{\beta} \end{bmatrix} \begin{Bmatrix} \dot{\bar{\alpha}} \\ \dot{\bar{\beta}} \\ \dot{\bar{\gamma}} \end{Bmatrix} . \tag{11}$$

And, making use of previously defined quantities, equation (10) can be compacted as,

$$\boldsymbol{\alpha}_k = \boldsymbol{\alpha}_c + \mathbf{R}_c \left(\bar{\mathbf{A}}_k \ddot{\bar{\boldsymbol{\theta}}}_k + \dot{\bar{\mathbf{A}}}_k \dot{\bar{\boldsymbol{\theta}}}_k \right) + \boldsymbol{\omega}_c \times \mathbf{R}_c \bar{\mathbf{A}}_k \frac{\mathrm{d}\bar{\boldsymbol{\theta}}_k}{\mathrm{d}\bar{z}_i} \dot{\bar{z}}_i \,. \tag{12}$$

where the term in parentheses contains both the first and second derivatives of $\bar{\boldsymbol{\theta}}_k$ with respect to $\bar{z}_i$, which are tabulated as functions of $\bar{z}_i$. The acceleration expressions provided in equations (9) and (12) are general. However, as mentioned before, the acceleration analysis is carried out for a virtual null value of the independent accelerations $\ddot{\mathbf{z}}$ and, hence, all the terms depending on $\ddot{\mathbf{z}}$ must be eliminated for this analysis.

It must be pointed out that, once the lookup tables are created at position level, the corresponding tables at velocity and acceleration level have been obtained by numerical differentiation through the central difference method. However, some additional comments must be done, as indicated is the previous section. For the front suspensions, knuckle position and orientation not only depends on the suspension coordinate, but also on the steering input, which means that time derivatives appearing in the previous equations should take such a dependence into account, while they did not. Conversely, what has been done is to generate a different lookup table of the front suspensions for each value of the steering input. This means that terms due to the variation in time of the steering input have been neglected in the calculation of the velocities and accelerations of the front knuckles. In the same way, for the rear suspension, the knuckle orientation not only depends on the suspension coordinate, but also on the vehicle roll angle. Corrections have been introduced to the lookup tables depending on such an angle, so that terms due to the roll rate have been neglected in the calculation of the velocities and accelerations of the rear knuckles.

Now, a new set of coordinates is defined, the so-called body coordinates, which can be expressed for each body at velocity level in the following form,

$$\mathbf{Z} = \begin{Bmatrix} \dot{\mathbf{s}} \\ \boldsymbol{\omega} \end{Bmatrix} . \tag{13}$$

being $\dot{\mathbf{s}}$ the velocity of the point of the body which at that particular time is coincident with the fixed frame origin, and $\boldsymbol{\omega}$ the angular velocity of the body. The relation between the body coordinates (and their time derivatives) of two neighbor bodies is,

$$\mathbf{Z}_i = \mathbf{Z}_{i-1} + \mathbf{b}_i \dot{\mathbf{z}}_i \,. \tag{14}$$

$$\dot{\mathbf{Z}}_i = \dot{\mathbf{Z}}_{i-1} + \mathbf{b}_i \ddot{\mathbf{z}}_i + \mathbf{d}_i \,. \tag{15}$$

Terms $\mathbf{b}_i$ and $\mathbf{d}_i$ are calculated in the same kinematic travelling of the chain mentioned above. Explicit expressions of $\mathbf{b}_i$ and $\mathbf{d}_i$ terms are available for conventional joints [3], and they have been used for the wheels, as they are connected to the knuckles through rotational joints. However, for the knuckles, connected to the chassis by means of macro-joints that substitute the suspension links, the following reasoning has been applied: terms $\mathbf{b}_i$ are nothing but the difference $\left(\mathbf{Z}_i - \mathbf{Z}_{i-1}\right)$ for a unit value of the relative joint velocity $\dot{\mathbf{z}}_i$; analogously, terms $\mathbf{d}_i$ are the difference $\left(\dot{\mathbf{Z}}_i - \dot{\mathbf{Z}}_{i-1}\right)$ for a null value of the relative joint acceleration $\ddot{\mathbf{z}}_i$. Therefore, classical velocity and acceleration relations, along with those provided before in this section, have been used to obtain the $\mathbf{b}_i$ and $\mathbf{d}_i$ terms for the knuckles. The chassis also requires a special comment: in this case, equation (14) relates the chassis body coordinates, $\mathbf{Z}_c$, with the six first coordinates of vector $\mathbf{z}$ and, hence, the $\mathbf{b}_i$ term is not a 6x1 vector but a 6x6 matrix, which has been called $\mathbf{B}_c$. The form of this matrix is the following,

$$\mathbf{B}_c = \begin{bmatrix} \mathbf{I}_{3x3} & \tilde{\mathbf{r}}_c \mathbf{A}_c \\ \mathbf{0}_{3x3} & \mathbf{A}_c \end{bmatrix} . \tag{16}$$

where $\tilde{\mathbf{r}}_c$ is the dual anti-symmetric matrix of vector $\mathbf{r}_c$, and $\mathbf{A}_c$ is the matrix that multiplies the vector of Cardan-angles derivatives to provide the chassis angular velocity, similar to matrix $\bar{\mathbf{A}}_k$ for the knuckles in equation (7). The $\mathbf{d}_i$ term for the chassis, $\mathbf{d}_c$, is obtained by classical kinematic relations and does not require any particular remark.

Once all the $\mathbf{b}_i$ and $\mathbf{d}_i$ terms have been evaluated, the following relationship between the relative and the body coordinates can be written,

$$\mathbf{Z} = \mathbf{R}\dot{\mathbf{z}} = \begin{bmatrix} \mathbf{B}_c & \mathbf{0} & \mathbf{0} & \mathbf{0} & \mathbf{0} & \mathbf{0} & \mathbf{0} & \mathbf{0} & \mathbf{0} \\ \mathbf{B}_c & \mathbf{b}_{k1} & \mathbf{0} & \mathbf{0} & \mathbf{0} & \mathbf{0} & \mathbf{0} & \mathbf{0} & \mathbf{0} \\ \mathbf{B}_c & \mathbf{0} & \mathbf{b}_{k2} & \mathbf{0} & \mathbf{0} & \mathbf{0} & \mathbf{0} & \mathbf{0} & \mathbf{0} \\ \mathbf{B}_c & \mathbf{0} & \mathbf{0} & \mathbf{b}_{k3} & \mathbf{0} & \mathbf{0} & \mathbf{0} & \mathbf{0} & \mathbf{0} \\ \mathbf{B}_c & \mathbf{0} & \mathbf{0} & \mathbf{0} & \mathbf{b}_{k4} & \mathbf{0} & \mathbf{0} & \mathbf{0} & \mathbf{0} \\ \mathbf{B}_c & \mathbf{b}_{k1} & \mathbf{0} & \mathbf{0} & \mathbf{0} & \mathbf{b}_{w1} & \mathbf{0} & \mathbf{0} & \mathbf{0} \\ \mathbf{B}_c & \mathbf{0} & \mathbf{b}_{k2} & \mathbf{0} & \mathbf{0} & \mathbf{0} & \mathbf{b}_{w2} & \mathbf{0} & \mathbf{0} \\ \mathbf{B}_c & \mathbf{0} & \mathbf{0} & \mathbf{b}_{k3} & \mathbf{0} & \mathbf{0} & \mathbf{0} & \mathbf{b}_{w3} & \mathbf{0} \\ \mathbf{B}_c & \mathbf{0} & \mathbf{0} & \mathbf{0} & \mathbf{b}_{k4} & \mathbf{0} & \mathbf{0} & \mathbf{0} & \mathbf{b}_{w4} \end{bmatrix} \dot{\mathbf{z}} \,. \tag{17}$$

where now $\mathbf{Z}$ includes the body coordinates of all the bodies of the mechanism. $\mathbf{B}_c$ is a 6x6 matriz, while the $\mathbf{b}_i$ are 6x1 vectors, so that the zero elements in equation (17) are also 6x1 vectors. Differentiating equation (17) with respect to time yields,

$$\dot{\mathbf{Z}} = \mathbf{R}\ddot{\mathbf{z}} + \dot{\mathbf{R}}\dot{\mathbf{z}} = \mathbf{R}\ddot{\mathbf{z}} + \begin{Bmatrix} \mathbf{d}_c \\ \mathbf{d}_c + \mathbf{d}_{k1} \\ \mathbf{d}_c + \mathbf{d}_{k2} \\ \mathbf{d}_c + \mathbf{d}_{k3} \\ \mathbf{d}_c + \mathbf{d}_{k4} \\ \mathbf{d}_c + \mathbf{d}_{k1} + \mathbf{d}_{w1} \\ \mathbf{d}_c + \mathbf{d}_{k2} + \mathbf{d}_{w2} \\ \mathbf{d}_c + \mathbf{d}_{k3} + \mathbf{d}_{w3} \\ \mathbf{d}_c + \mathbf{d}_{k4} + \mathbf{d}_{w4} \end{Bmatrix} . \tag{18}$$

The special form of matrix $\mathbf{R}$, which can be written as the product of a connectivity and a diagonal matrix, allows to recursively accumulate the body mass matrices and forces from the leaves to the root of the kinematic chain [3]. The equations of motion expressed in body coordinates are projected into the independent relative coordinates by using equations (17) and (18), thus yielding,

$$\mathbf{R}^{\mathrm{T}}\bar{\mathbf{M}}\mathbf{R}\ddot{\mathbf{z}} = \mathbf{R}^{\mathrm{T}}\left(\bar{\mathbf{Q}} - \bar{\mathbf{M}}\dot{\mathbf{R}}\dot{\mathbf{z}}\right) . \tag{19}$$

where $\bar{\mathbf{M}}$ and $\bar{\mathbf{Q}}$ are the mass matrix and force vector of the system for body coordinates. Equation (19) can be further reduced to,

$$\mathbf{M}\ddot{\mathbf{z}} = \mathbf{Q} . \tag{20}$$

being $\mathbf{M}$ and $\mathbf{Q}$ the mass matrix and force vector for relative coordinates, whose expressions are,

$$\mathbf{M} = \begin{bmatrix} \mathbf{B}_c^{\mathrm{T}}\mathbf{M}_c\mathbf{B}_c & \mathbf{B}_c^{\mathrm{T}}\mathbf{M}_{k1}\mathbf{b}_{k1} & \mathbf{B}_c^{\mathrm{T}}\mathbf{M}_{k2}\mathbf{b}_{k2} & \mathbf{B}_c^{\mathrm{T}}\mathbf{M}_{k3}\mathbf{b}_{k3} & \mathbf{B}_c^{\mathrm{T}}\mathbf{M}_{k4}\mathbf{b}_{k4} & \mathbf{B}_c^{\mathrm{T}}\mathbf{M}_{w1}\mathbf{b}_{w1} & \mathbf{B}_c^{\mathrm{T}}\mathbf{M}_{w2}\mathbf{b}_{w2} & \mathbf{B}_c^{\mathrm{T}}\mathbf{M}_{w3}\mathbf{b}_{w3} & \mathbf{B}_c^{\mathrm{T}}\mathbf{M}_{w4}\mathbf{b}_{w4} \\ & \mathbf{b}_{k1}^{\mathrm{T}}\mathbf{M}_{k1}\mathbf{b}_{k1} & \mathbf{0} & \mathbf{0} & \mathbf{0} & \mathbf{b}_{k1}^{\mathrm{T}}\mathbf{M}_{w1}\mathbf{b}_{w1} & \mathbf{0} & \mathbf{0} & \mathbf{0} \\ & & \mathbf{b}_{k2}^{\mathrm{T}}\mathbf{M}_{k2}\mathbf{b}_{k2} & \mathbf{0} & \mathbf{0} & \mathbf{0} & \mathbf{b}_{k2}^{\mathrm{T}}\mathbf{M}_{w2}\mathbf{b}_{w2} & \mathbf{0} & \mathbf{0} \\ & & & \mathbf{b}_{k3}^{\mathrm{T}}\mathbf{M}_{k3}\mathbf{b}_{k3} & \mathbf{0} & \mathbf{0} & \mathbf{0} & \mathbf{b}_{k3}^{\mathrm{T}}\mathbf{M}_{w3}\mathbf{b}_{w3} & \mathbf{0} \\ & & & & \mathbf{b}_{k4}^{\mathrm{T}}\mathbf{M}_{k4}\mathbf{b}_{k4} & \mathbf{0} & \mathbf{0} & \mathbf{0} & \mathbf{b}_{k4}^{\mathrm{T}}\mathbf{M}_{w4}\mathbf{b}_{w4} \\ & & & & & \mathbf{b}_{w1}^{\mathrm{T}}\mathbf{M}_{w1}\mathbf{b}_{w1} & \mathbf{0} & \mathbf{0} & \mathbf{0} \\ & \text{sym.} & & & & & \mathbf{b}_{w2}^{\mathrm{T}}\mathbf{M}_{w2}\mathbf{b}_{w2} & \mathbf{0} & \mathbf{0} \\ & & & & & & & \mathbf{b}_{w3}^{\mathrm{T}}\mathbf{M}_{w3}\mathbf{b}_{w3} & \mathbf{0} \\ & & & & & & & & \mathbf{b}_{w4}^{\mathrm{T}}\mathbf{M}_{w4}\mathbf{b}_{w4} \end{bmatrix} . \tag{21}$$

where $\mathbf{M}_{wi} = \bar{\mathbf{M}}_{wi}$, $\mathbf{M}_{ki} = \bar{\mathbf{M}}_{ki} + \mathbf{M}_{wi}$, and $\mathbf{M}_{c} = \bar{\mathbf{M}}_{c} + \mathbf{M}_{k1} + \mathbf{M}_{k2} + \mathbf{M}_{k3} + \mathbf{M}_{k4}$, being the terms with an upper bar the basic body mass matrices,

$$\mathbf{Q} = \begin{Bmatrix} \mathbf{B}_{c}^{T}\mathbf{Q}_{c} \\ \mathbf{b}_{k1}^{T}\mathbf{Q}_{k1} \\ \mathbf{b}_{k2}^{T}\mathbf{Q}_{k2} \\ \mathbf{b}_{k3}^{T}\mathbf{Q}_{k3} \\ \mathbf{b}_{k4}^{T}\mathbf{Q}_{k4} \\ \mathbf{b}_{w1}^{T}\mathbf{Q}_{w1} \\ \mathbf{b}_{w2}^{T}\mathbf{Q}_{w2} \\ \mathbf{b}_{w3}^{T}\mathbf{Q}_{w3} \\ \mathbf{b}_{w4}^{T}\mathbf{Q}_{w4} \end{Bmatrix} \quad \text{with} \quad \begin{aligned} \mathbf{Q}_{wi} &= \bar{\mathbf{Q}}_{wi} - \bar{\mathbf{M}}_{wi}\left(\mathbf{d}_{c} + \mathbf{d}_{ki} + \mathbf{d}_{wi}\right) \\ \mathbf{Q}_{ki} &= \bar{\mathbf{Q}}_{ki} - \bar{\mathbf{M}}_{ki}\left(\mathbf{d}_{c} + \mathbf{d}_{ki}\right) + \mathbf{Q}_{wi} \\ \mathbf{Q}_{c} &= \bar{\mathbf{Q}}_{c} - \bar{\mathbf{M}}_{c}\mathbf{d}_{c} + \mathbf{Q}_{k1} + \mathbf{Q}_{k2} + \mathbf{Q}_{k3} + \mathbf{Q}_{k4} \end{aligned} . \tag{22}$$

being the terms with an upper bar the basic body forces.

To integrate in time the ODE provided by equation (20), the implicit single-step trapezoidal rule with fixed time step has been adopted. Combination of the integrator equations with the equations of motion (20), taking the positions as primary variables, leads to a nonlinear system of equations $\mathbf{f}\left(\mathbf{z}_{n+1}\right) = 0$, where $\mathbf{z}_{n+1}$ is the vector of independent coordinates at the next time step, which can be solved by means of a Newton-Raphson iteration procedure, being the residual vector and the approximated tangent matrix,

$$\mathbf{f}\left(\mathbf{z}\right) = \frac{\Delta t^2}{4}\left(\mathbf{M}\ddot{\mathbf{z}} - \mathbf{Q}\right). \tag{23}$$

$$\frac{\partial \mathbf{f}\left(\mathbf{z}\right)}{\partial \mathbf{z}} = \mathbf{M} + \frac{\Delta t}{2}\mathbf{C} + \frac{\Delta t^2}{4}\mathbf{K}. \tag{24}$$

where $\mathbf{K} = -\partial\mathbf{Q}/\partial\mathbf{z}$ and $\mathbf{C} = -\partial\mathbf{Q}/\partial\dot{\mathbf{z}}$ represent the contribution of damping and elastic forces to the tangent matrix, and Δt is the time step.

4 Tests and results

The objective of the tests is to compare the behavior of the car conventional and motor in-wheel configurations so as to assess whether the second option may present negative effects on ride, handling and steering characteristics due to the increase in unsprung mass.

As ride characteristics, impact feel and pitch control have been considered, which can be measured through chassis vertical acceleration and pitch angle histories, respectively, during a sine sweep test (ISO 2631: 2004). In this test, the car is driven at a constant speed of 40 km/h over the road profile shown in figure 4, whose analytical expression is provided in equation (25), with A = 0.13 m, λ = 0.016, ω = 1.5 rad/m, X = 210 m.

$$z(x) = A\,\mathrm{e}^{-\lambda x}\sin\frac{\omega x^2}{X}. \tag{25}$$

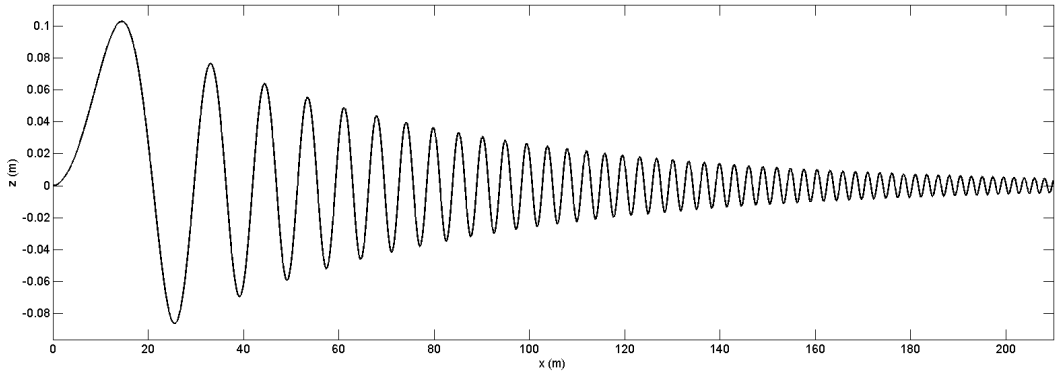

Figure 4. Sine sweep test.

The resulting chassis vertical acceleration and pitch angle histories have been measured and are gathered in figure 5. Almost no difference is perceived in the pitch angle history between both configurations. However, a slightly higher vertical acceleration is observed at high frequencies of excitation for the in-wheel configuration, which would translate in a worse behavior of that alternative from the comfort point of view.

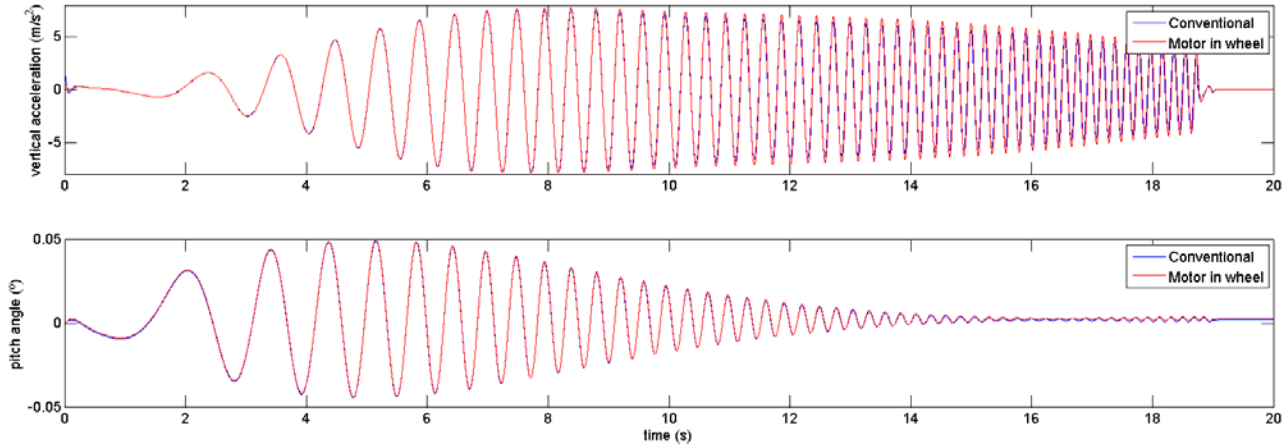

Figure 5. Histories of chassis vertical acceleration and pitch angle in the sine sweep test.

Regarding handling characteristics, stability can be deducted from the histories of yaw and roll angles in an obstacle avoidance test (ISO 3888: 2002), illustrated in figure 6. To carry out the simulations, an analytical function has been defined describing the ideal car trajectory. The function is composed of straight segments for the initial and final parts of the maneuver and of cicloidal curves for the central part of the maneuver. Then, a simple proportional controller has been implemented, which introduces a steering input to correct the drift of a point in the center of the vehicle's front axle with respect to the ideal trajectory. Entrance speeds to the test were increased until unstable behavior was reached. The maximum acceptable entrance speed was 43 km/h. Figure 7 shows the resulting histories of yaw angle drift from the tangent to the ideal trajectory and roll angle, for the conventional and motor in-wheel configurations. The histories of the first angle are almost identical for both configurations, while a slightly higher roll angle can be appreciated for the motor in-wheel configuration, which indicates less stable behavior.

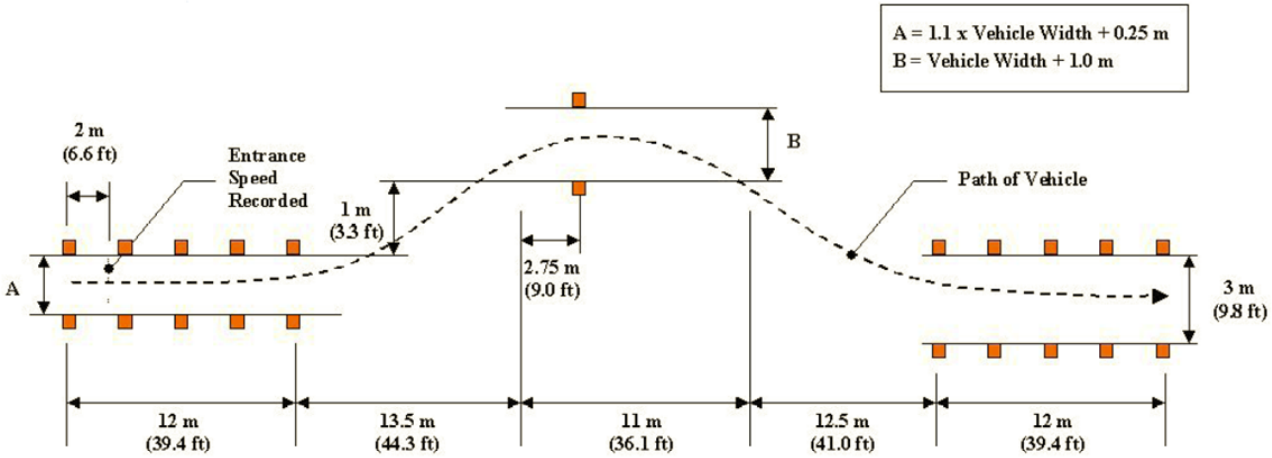

Figure 6. Obstacle avoidance test.

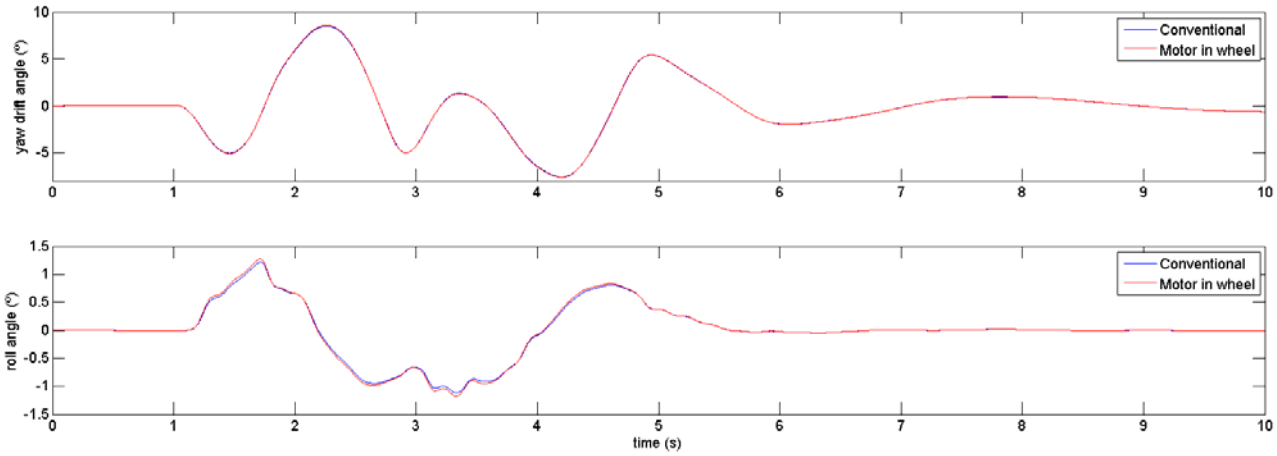

Figure 7. Histories of yaw drift angle and roll angle in the obstacle avoidance test.

Still looking at handling characteristics, under/oversteer balance can be determined from a handling diagram in a constant radius test (ISO 4138: 2004). In the same test, steering characteristics -effort level and linearity-, can also be measured. For this test, a circle of radius 100 m has been considered. The same simple proportional controller described in the previous test has been implemented to mimic the driver's action. The car started from rest, tangent to the trajectory, and its speed was progressively increased by the introduction of a 125 Nm torque in each of the front wheels. The test was terminated when unstable behavior was detected, which took place at an approximate speed of 100 km/h for both configurations (figure 8). Due to the higher total mass (30 kg in each front wheel), the motor in-wheel configuration required more time to reach the critical speed. Figure 9 shows the handling diagram obtained from the test for the conventional and motor in-wheel configurations. Figure 10 presents the required steering effort in both cases. A mild understeer behavior is observed in the handling diagram, while the steering effort keeps linear after the initial transient phase until the critical speed is reached. Both configurations yield almost identical results.

To give an idea of the developed code efficiency, table 2 shows the duration of each simulated test along with the CPU-time required to execute the simulation on a Intel Core i7 950 @ 3.07 GHz. The fixed time step of integration for all the simulations is Δt = 1 ms.

Table 2. Code efficiency.

Test	*Simulation* (s)	*CPU-time* (s)
Sine sweep	20	1.272
Obstacle avoidance	10	0.614
Constant radius	60	1.851

Figure 8. Critical conditions in the constant radius test.

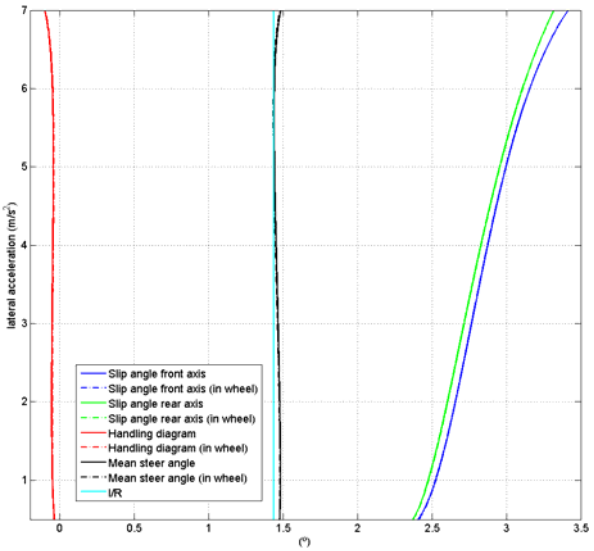

Figure 9. Handling diagram from the constant radius test.

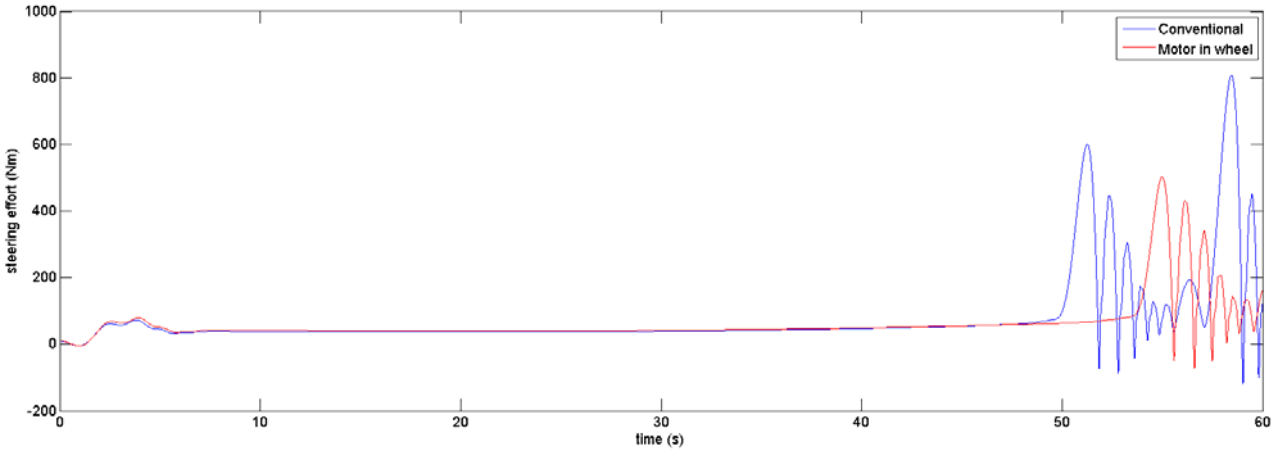

Figure 10. Steering effort in the constant radius test.

5 Conclusion

Motor in-wheel configuration presents advantages for electric-powered vehicles over conventional standalone motor configuration, like improved modularity when designing different drivetrains (FWD, RWD, AWD) and increased usable interior space of the vehicle. However, the increased unsprung mass can lead to drawbacks in ride and/or handling behavior and represents a challenge for suspension designers since no previous similar data are available.

To compare the dynamic behavior of conventional and motor in-wheel configurations, a typical B-segment car, a Fiat Punto, has been modeled, and subject to three simulated tests so as to obtain indicators of ride, handling and steering characteristics. The motor in-wheel has been modeled by adding a point mass of 30 kg in each one of the front wheels. The car suspensions have been considered as macro-joints whose kinematics are provided by means of lookup tables, thus streamlining the introduction of suspension changes as substitution of the corresponding table is only needed. A robust and efficient semi-recursive dynamic formulation in independent relative coordinates with numerical integration by means of the trapezoidal rule has been developed, so that violent maneuvers can be carried out in very short times, even allowing to perform hardware-in-the-loop simulations if required.

Results gathered from the three tests -sine sweep, obstacle avoidance and constant radius- reveal that handling and steering characteristics of the motor in-wheel configuration are similar to those of the conventional one, while ride is slightly degraded, particularly at high frequencies of excitation.

Future research will investigate the behavior degradation of the motor in-wheel configuration when wheels lose contact with the ground, i.e. in the presence of bumps or holes, as well as the application of the model for the development of torque control strategies for improved vehicle handling.

References

[1] EARPA Position Paper: Research and innovation on hybrid and electric components & systems, towards Horizon 2020. `http://www.earpa.eu`, November 2012.

[2] M. Anderson, D. Harty. Unsprung mass with in-wheel motors – myths and realities. In *Proceedings of the 10th Int. Symposium on Advanced Vehicle Control (AVEC 10)*, Loughborough, UK, 2010.

[3] J. Cuadrado, D. Dopico, M. Gonzalez, M.A. Naya, A combined penalty and recursive real-time formulation for multibody dynamics, *Journal of Mechanical Design*, 126(4):602-608, 2004.

[4] M. Acevedo, J.T. Celigüeta, Real-time dynamic simulation of passenger cars. In *Proceedings of the 27th ISATA on Mechatronics & Supercomputing Applications in the Transportation Industries*, pp. 559-566, Aachen, Germany, 1994.

[5] W.F. Milliken, D.L. Milliken, *Race car vehicle dynamics*, SAE International, 1994.